Phase Equilibria in the Quaternary Molybdenum-Ruthenium-Rhodium-Palladium System

J. Octavio A. Paschoal*, Heiko Kleykamp, and Fritz Thümmler

(Kernforschungszentrum Karlsruhe, Institut für Material- und Festkörperforschung, Postfach 3640, D-7500 Karlsruhe)

The phase behaviour of the quaternary Mo-Ru-Rh-Pd system and the four ternary Mo-Ru-Rh, Mo-Ru-Pd, Mo-Rh-Pd and Ru-Rh-Pd systems has been investigated at 1700 °C. The quaternary system is characterized by the hcp ε-Ru(Mo,Rh,Pd) solid solution which can dissolve up to 48 at.% bcc Mo, 60 at.% fcc Rh and 15 at.% fcc Pd, resp. The intermediate hcp phases in the binary Mo-Rh and Mo-Pd systems are stabilized in the range of 43 to 82 at.% Rh and 51 to 53 at.% Pd, resp., and form continuous solid solutions with ε-Ru(Mo,Rh,Pd). Up to 5 at.% Rh and 5 at.% Pd, resp., can be dissolved in the σ-phase Mo_5Ru_3. Fcc α-Rh(Mo,Ru,Pd) can dissolve up to 14 at.% Mo, 34 at.% Ru and 47 at.% Pd in the respective binary boundary systems. Complete miscibility exists between Rh and the fcc α region of the binary Mo-Pd system (approx. 60 to 70 at.% Pd at 1700 °C), whereas Rh can dissolve up to 80 at.% $Ru_{0.5}Pd_{0.5}$. Lattice parameter and Vickers hardness results of the solid solution regions and pseudoternary sections of the quaternary system are given.

Der Aufbau des Vierstoffsystems Molybdän-Ruthenium-Rhodium-Palladium

Der Aufbau des Vierstoffsystems Mo-Ru-Rh-Pd und der vier ternären Randsysteme Mo-Ru-Rh, Mo-Ru-Pd, Mo-Rh-Pd und Ru-Rh-Pd bei 1700 °C wird beschrieben. Das Vierstoffsystem wird durch die hexagonale ε-Phase der festen Lösung Ru(Mo,Rh,Pd) bestimmt, die in den entsprechenden binären Systemen 48 % krz Mo, 60 % kfz Rh bzw. 15 % kfz Pd aufnehmen kann (Werte in At.-%). In den binären Randsystemen Mo-Rh und Mo-Pd werden intermediäre hexagonale Phasen mit 43 bis 82 % Rh bzw. mit 51 bis 53 % Pd stabilisiert, die mit ε-Ru(Mo,Rh,Pd) lückenlose Mischkristalle bilden. Die im System Mo-Ru beobachtete σ-Phase Mo_5Ru_3 kann 5 % Rh bzw. 5 % Pd lösen. Die kfz α-Phase der festen Lösung Rh(Mo,Ru,Pd) kann in den entsprechenden binären Systemen 14 % Mo, 34 % Ru bzw. 47 % Pd aufnehmen. Zwischen Rh und der kfz α-Phase im binären Randsystem Mo-Pd (etwa 60 bis 70 % Pd bei 1700 °C) besteht vollständige Mischbarkeit, während bis zu 80 % $Ru_{0.5}Pd_{0.5}$ in Rh gelöst werden können. Die Gitterkonstanten und die Vickershärte der Mischkristallphasen sowie pseudoternäre Schnitte des quaternären Systems werden mitgeteilt.

1. Introduction

$(U_{1-y}Pu_y)O_{2-x}$ mixed oxide (MOX) is used as fuel material in fast breeder reactors; the cladding of the pins being an austenitic steel. Various fission products are generated during burnup which alter the chemical and mechanical properties of the fuel. Furthermore, on account of the high temperature gradient in the fuel that exists during operation, the fission products can migrate to the cladding and interact chemically. The oxygen potential of the MOX characterized by the oxygen-to-metal ratio is an important parameter for the chemical behaviour of the fuel during operation. It has a major influence on the reactions that occur under irradiation between the fuel, fission products, cladding components and in the case of cladding failure, the sodium coolant.

Postirradiation examinations of MOX reveal that a group of fission products is present as five-component metallic precipitates. These so-called "white inclusions" contain molybdenum, technetium, ruthenium, rhodium and palladium[1] to [5]. The composition of these alloys varies considerably and depends on the fission yield, the initial O/(U+Pu) ratio of the fuel, the temperature gradient in the pin and the burnup[6][7]. The Mo concentration in the alloys decreases by oxidation of this element due to an increase of the oxygen potential of the MOX with burnup. This is effected by delivering oxygen as a result of the fission process because this element cannot completely be bonded by the generated fission products[8][9]. On the other hand, the alloys become two-phase at low oxygen potentials and high Mo fractions as it has been observed in coated particles of high temperature reactor fuels[10][11], in light water reactor fuels[12], or in defective fast breeder reactor MOX fuels[13]. The ratio of the Mo concentration in the "white inclusions" to the MoO_2 concentration in the multi-component Mo oxide precipitates[8] is an indicator of the local oxygen potential of MOX:

$$[Mo]_{alloy} + O_2 = [MoO_2]_{ceramic\ phase}$$

Therefore, the information on the constitution of the five-component Mo-Tc-Ru-Rh-Pd system is important for the interpretation of numerous phenomena in irradiated MOX.

The phase diagrams of the two-component systems between Mo, Ru, Rh and Pd have been reviewed in [14][15][16]. No experimental results were available about the Ru-Rh system. However, this lacuna has been filled up recently by phase studies between 800 and 2400 °C[16]. Phase studies in the Tc-Ru system were published by Darby et al.[17][18]. Haines et al.[19] have used a computer programme to sketch the binary Mo-Tc, Tc-Rh and Tc-Pd systems as well as isothermal sections at 1800, 2000 and 2200 K of the ternary Mo-Tc-Rh, Mo-Tc-Pd and Mo-Ru-Pd systems. Rand and Potter[20] gave improved isothermal sections at 1800 and 2000 K of the ternary Mo-Ru-Rh system by computer calculations. No experimental results are known about the ternary systems. Thermodynamic investigations in the

* Delegated from the Instituto de Pesquisas Energéticas e Nucleares, Sao Paulo, Brasil.

Mo-Rh, Mo-Pd and Mo-Ru-Pd systems have been carried out so far by Yamawaki et al.[21]) in the temperature range of 1200 to 1300 K.

The objective of this work is the experimental study of isothermal sections at 1700 °C in the ternary Mo-Ru-Rh, Mo-Ru-Pd, Mo-Rh-Pd and Ru-Rh-Pd systems as well as in the quaternary Mo-Ru-Rh-Pd system[16]). The β active hcp Tc which is completely miscible with Ru[17])[18]) has not been used in these laboratory studies. The results should provide a better insight into the phase behaviour of the five-component Mo-Tc-Ru-Rh-Pd system and the chemical

Table 1. Lattice parameters of the elements used in this study.

element	structure	lattice parameters in pm	
		literature values[22])	used material
Mo	bcc	$a = 314.70$	$a = 314.4 \pm 0.1$
Ru	hcp	$a = 270.58$ $c = 428.11$	$a = 270.4 \pm 0.1$ $c = 427.8 \pm 0.1$
Rh	fcc	$a = 380.36$	$a = 380.4 \pm 0.1$
Pd	fcc	$a = 389.08$	$a = 388.8 \pm 0.1$

Table 2. Compositions and lattice parameters of phases in the Mo-Ru-Rh system.

nominal comp. in at.%			phases	lattice parameters in pm			EMPA results in at.%		
Mo	Ru	Rh		a	c	c/a	Mo	Ru	Rh
10	63	27	ε	272.0	430.8	1.584	9.0	62.9	28.1
10	50	40	ε	272.0	431.6	1.587	-	-	-
15	35	50	ε	272.8	433.7	1.590	-	-	-
20	20	60	ε	272.5	434.2	1.594	-	-	-
30	30	40	ε	274.2	436.6	1.592	-	-	-
33.3	46.7	20	ε	274.5	437.8	1.595	32.0	47.9	20.1
45	38.5	16.5	ε	275.2	441.5	1.604	43.8	40.4	15.8
50	35	15	ε	276.1	443.6	1.607	-	-	-
			σ	956.7	493.4	0.516	-	-	-
50	15	35	ε	276,1	443,7	1,607	-	-	-
52	28.5	19.5	ε	276.2	443.8	1.607	-	-	-
			σ	956.4	494.8	0.517	-	-	-
55	10	35	ε	276.3	444.0	1.607	54.9	10.5	34.5
57	24	19	ε	276.6	443.4	1.603	-	-	-
			σ	956.3	495.2	0.518	-	-	-
			β	314.2					
60	10	30	ε	276.6	444.9	1.609	-	-	-
			β	314.1					
60.7	27.8	11.5	ε	276.2	443.2	1.605	53.8	27.6	18.6
			β	313.4			78.6	16.5	4.9
			σ (*)	960.0	492.0	0.512	-	-	-
65.9	20.1	14.0	ε	276.1	443.4	1.606	53.0	26.3	20.7
			β	313.5			78.3	14.3	7.4
			σ (+)	-	-	-	-	-	-
65	15	20	ε	275.9	443.8	1.609	-	-	-
			β	313.7					
			σ	956.5	496.0	0.519	-	-	-
69.5	11.0	19.5	ε	276.3	444.0	1.607	-	-	-
			β	313.8					
75	20	5	ε	275.9	442.9	1.605	53.3	33.1	13.6
			β	313.4			76.7	19.1	4.2
			σ	959.1	494.6	0.516	-	-	-
78.5	11	10.5	ε	276.8	444.0	1.604	-	-	-
			β	313.8			78.3	11.8	9.9

(*) lattice parameters calculated from two reflections

(+) only one reflection

phenomena related to the chemical state of these fission products in irradiated MOX. A temperature of 1700 °C has been taken in this investigation because the phase behaviour of Pd should be studied in particular above its melting point (1555 °C). A temperature higher than 1700 °C would have led to difficulties with respect to incompatibilities with the container material during heat treatment.

2. Experimental work

Samples for the phase studies were prepared from the elements (purity ≧ 99.7 %). The lattice parameters of the powders used are shown in table 1. The powder mixtures were compacted in a steel die and molten in an arc-furnace under argon atmosphere. The samples were then homogenized at 1700 °C in high vacuum (≈ 10^{-8} bar) for periods between 20 and 100 h. The temperature was controlled by means of a calibrated pyrometer. All samples were weighed before and after heat treatment; those with weight losses higher than 10 % were discarded. Alloys with high Pd contents were encapsulated under argon in tantalum crucibles before heat treatment because of the high Pd vapour pressure. The cooling rate by flushing with argon was limited due to the used furnace type to about 550 K/min in the temperature range of 1700 °C down to 800 °C.

The samples were analyzed metallographically and by X-ray diffraction, electronprobe microanalysis (EPMA) and microhardness measurements. Light-optical and electron-optical images were prepared from embedded and polished specimens. Optical contrast between the phases was achieved by different etching reagents. Mo rich specimens were etched with an aqueous NaOH-$K_3Fe(CN)_6$ solution; Ru rich specimens were gas etched; Rh and Pd rich specimens were etched with boiling aqua regia; in some cases polarized light was used. Standard Guinier procedures (Cu-Kα_1 radiation) were applied for the X-ray diffraction analysis of the powdered material. EPMA has been performed by a Cameca MS 46 instrument. The measured intensities of the components have been corrected to weight and mole fractions, resp., by use of a ZAF computer programme. Vickers hardness measurements have been performed with a load of 1 N. The diagonals of indentation were calculated automatically to HV values. The given results are an averaged value of approximately 20 indentations within the respective sample region.

3. Results and discussion

3.1 The ternary Mo-Ru-Rh system

The nominal compositions of the investigated samples as well as the X-ray analysis and the EPMA results are compiled in table 2. The phases denoted ε, α and β correspond to the host lattice of the hexagonal Ru, the fcc Rh and Pd, and the bcc Mo, resp. The phase designated σ corresponds to the tetragonal Mo_5Ru_3 phase which occurs in the binary Mo-Ru system. The phase boundaries are essentially based on the EPMA results. Typical microstructures are shown in fig. 1. The dark regions in figs. 1a and b are related to the β phase (Mo rich solid solution). The light

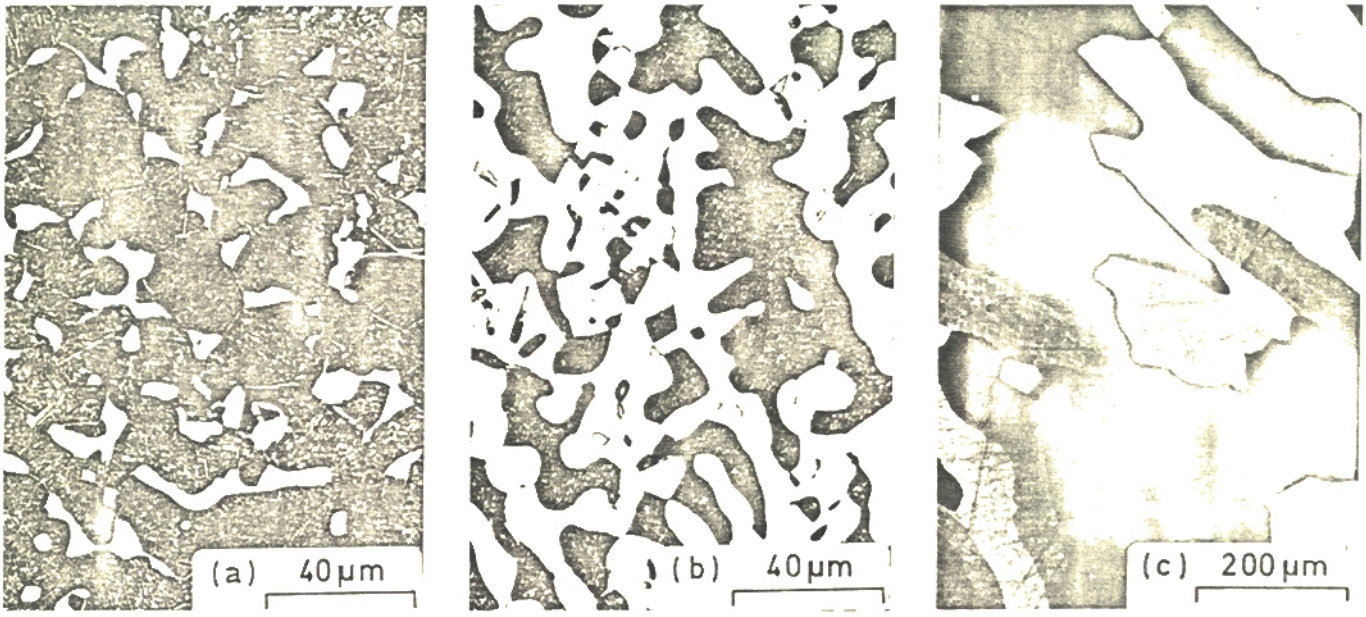

Fig. 1a to c. Microstructures of alloys in the Mo-Ru-Rh system after annealing at 1700 °C. (a) 75 Mo, 20 Ru, 5 Rh (at.%); dark: $\beta + \varepsilon$, bright: ε. (b) 65.9 Mo, 20.1 Ru, 14.0 Rh; dark: $\beta + \varepsilon$, bright: ε, σ observed by X-ray diffraction. (c) 9.0 Mo, 62.9 Ru, 28.1 Rh; mono-phase: ε *(polarized light)*.

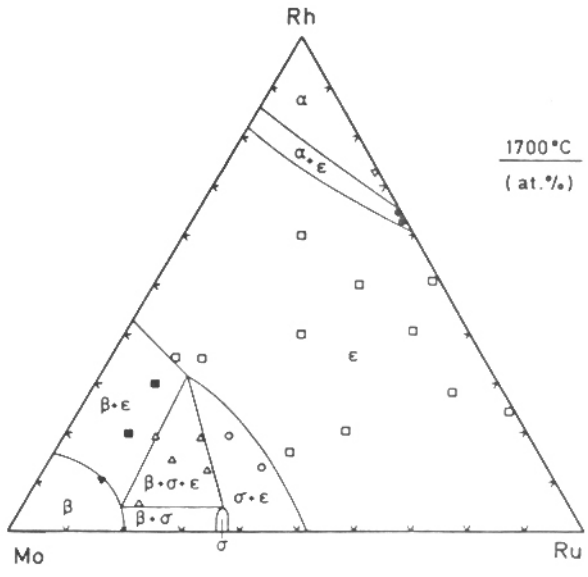

Fig. 2. Isothermal section of the ternary Mo-Ru-Rh system at 1700 °C.

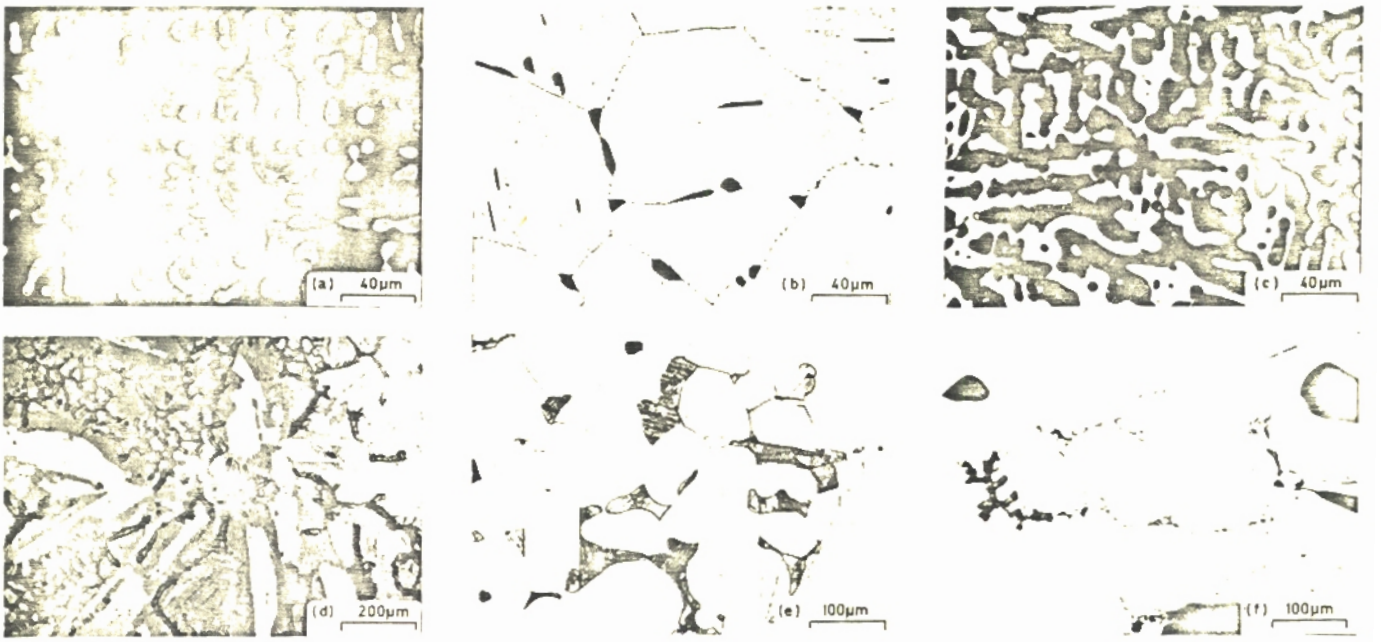

Fig. 3a to f. Microstructures of alloys in the Mo-Ru-Pd system after annealing at 1700 °C. (a) 77.5 Mo, 10.4 Ru, 12.1 Pd (at.%); dark: $\beta + \varepsilon$, bright: ε. (b) 50 Mo, 5 Ru, 45 Pd; dark phases at grain boundaries: $\beta + \varepsilon$; bright: ε, β partly precipitated during cooling. (c) 66.6 Mo, 19.8 Ru, 13.6 Pd; dark: $\beta + \varepsilon$, bright: ε, σ observed by X-ray diffraction. (d) 20 Mo, 20 Ru, 60 Pd; bright: ε, grey: α, dark network: liquid. (e) 25 Mo, 25 Ru, 50 Pd; bright: ε, dark: α. (f) 15 Mo, 30 Ru, 55 Pd; bright: ε, grey phases at grain boundaries: liquid.

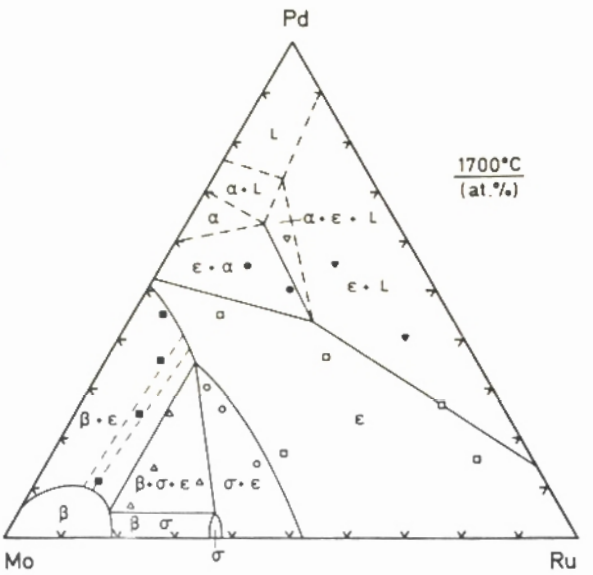

Fig. 4. Isothermal section of the ternary Mo-Ru-Pd system at 1700 °C.

needles within the dark β phase are ε phase precipitates formed during cooling from the liquid. The σ phase could be identified definitely only by X-ray analysis and by EPMA; however, metallographic observation was possible in samples with high σ phase fraction. Typical microstructures of the σ phase are shown in figs. 11c and d for samples from the quaternary Mo-Ru-Rh-Pd system.

In the binary Mo-Ru system, there is a high Mo solubility in Ru, which is extended up to 48 at.% Mo at 1700 °C[23][24]). An intermediate hexagonal ε phase with a broad homogeneity range between 43 and 82 at.% Rh is stabilized in the binary Mo-Rh system[23][25][26]). Intermediate phases of such a kind are found in those systems where an element of the Vb and VIb transition metal group with a bcc structure is alloyed with an fcc element of the VIIIb or VIIIc subgroup[27][28]). There were no published experimental results on the phase diagram of the binary Ru-Rh system. Recent investigations[16]) elucidated high mutual solubilities which, as determined by EPMA give up to 60.0 at.% Rh in Ru and up to 34.5 at.% Ru in Rh, resp., at 1700 °C[29]). Complete miscibility exists between the Ru(Mo,Rh) region and the intermediate ε phase of the Mo-Rh system. The tetragonal σ phase which exists in the binary Mo-Ru system in a narrow concentration range (about (37 ± 1) at.% Ru, probably Mo_5Ru_3[23][24])) is stabilized by Rh additions up to 5 at.%. An increase in the stability of the σ phase in the Mo-Ru system by other ternary additives, such as Re[30]) and V[31]) has been already established.

The isothermal section of the ternary Mo-Ru-Rh system at 1700 °C is given in fig. 2. The system is characterized by a continuous solid solution region between the hexagonal Ru and the stabilized ε phase of the binary Mo-Rh system (microstructure in fig. 1c). The c/a ratio is markedly increased with growing Mo content from 1.583 for pure Ru to 1.609 for the Mo rich solid solution in equilibrium with the β phase (table 2).

3.2 The ternary Mo-Ru-Pd system

The nominal compositions of the investigated samples as well as the X-ray analysis and the EPMA results are summarized in table 3. Typical microstructures are given in fig. 3. The unetched bright areas correspond to the ε phase. The etched dark regions in figs. 3a and b are $\beta + \varepsilon$ phases. The σ phase of the three-phase sample in fig. 3c could be observed unequivocally only by X-ray diffraction and by EPMA. Figures 3e and f represent samples from the two-phase $\varepsilon + \alpha$ and $\varepsilon +$ L regions, fig. 3d from the three-phase $\alpha + \varepsilon +$ L region. The phase denoted with L corresponds to the liquid phase at 1700 °C with high Pd contents forming a network around the grain boundaries of the ε phase.

Table 3. Compositions and lattice parameters of phases in the Mo-Ru-Pd system.

nominal comp. in at.%			phases	lattice parameters in pm			EMPA results in at.%		
Mo	Ru	Pd		a	c	c/a	Mo	Ru	Pd
10	75	15	ε	272.3	432.4	1.588	-	-	-
10	63	27	ε	272.7	433.1	1.588	-	-	-
15	30	55	ε	274.3	439.1	1.601	19.8	46.7	33.5
			α	387.7			12.8	10.4	76.8
20	20	60	ε	275.1	442.1	1.607	24.4	32.1	43.5
			α	388.8			24.0	12.8	63.2
			α_L (x)	-			15.6	11.4	73.0
25	25	50	ε	275.8	443.3	1.607	27.3	27.5	45.2
			α	388.1					
25	35	40	ε	275.1	440.4	1.601	26.9	36.5	36.6
30	15	55	ε	276.4	444.1	1.607	-	-	-
			α	388.7			-	-	-
40	15	45	ε	277.1	444.4	1.604	40.6	15.7	43.7
45	38.5	16.5	ε	276.5	443.7	1.605	42.0	42.4	15.6
48.4	37.0	14.6	ε	276.3	444.4	1.608	46.7	37.6	15.7
			σ	957.1	495.9	0.518	-	-	-
48.5	25.5	26.0	ε	276.4	444.0	1.606	-	-	-
			σ	957.9	495.0	0.517	-	-	-
49.5	20.5	30.0	ε	276.9	444.5	1.606	-	-	-
			σ	956.7	494.6	0.517	-	-	-
50	5	45	ε	277.5	444.7	1.603	46.7	5.9	47.4
			β	313.8			-	-	-
55	10	35	ε	277.3	444.4	1.603	48.4	10.8	40.8
			β	313.8			80.9	8.8	10.3
58.5	16.5	25	ε	276.6	443.6	1.604	-	-	-
			β	313.7	-	-	-	-	-
			σ (+)	-	-	-	-	-	-
60.6	28.5	10.9	ε	276.8	443.6	1.603	48.6	35.9	15.5
			β	313.0			77.3	18.3	4.4
			σ	956.3	494.0	0.517	-	-	-
64.0	11.5	24.5	ε	276.9	443.8	1.603	-	-	-
			β	313.4			-	-	-
66.6	19.8	13.6	ε	276.3	442.5	1.605	49.7	26.5	23.8
			β	312.9			78.5	15.1	6.4
			σ	956.2	494.2	0.517	-	-	-
75.0	20.0	5.0	ε	276.5	443.6	1.604	-	-	-
			β	313.6			78.8	15.8	5.4
			σ (*)	961.2	493.5	0.513	-	-	-
77.5	10.4	12.1	ε	276.8	444.0	1.604	49.6	13.9	36.5
			β	313.8			80.4	10.0	9.6

(*) lattice parameters calculated from two reflections

(+) only one reflection (x) liquid phase at 1700°C

An intermediate hexagonal ε phase with a small homogeneity range between 51 and 53 at.% Pd is stabilized in the binary Mo-Pd system at high temperatures[28]). The solubility of Pd in Ru is about 15 at.% Pd at 1700 °C[32])[33]). Complete miscibility exists between the hexagonal Ru(Mo,Pd) region and the intermediate ε phase of the Mo-Pd system. Again, the tetragonal σ phase existing in the Mo-Ru system is stabilized by Pd additions up to 5 at.%.

The isothermal section of the ternary Mo-Ru-Pd system at 1700 °C is illustrated in fig. 4. The system, similar to the Mo-Ru-Rh system, is characterized by a continuous solid solution region between the hexagonal Ru and the stabi-

Table 4. Compositions and lattice parameters of phases in the Mo-Rh-Pd system.

nominal comp. in at.%			phases	lattice parameters in pm			EPMA results in at.%		
Mo	Rh	Pd		a	c	c/a	Mo	Rh	Pd
10	45	45	α	380.2			12.9	44.0	43.1
			α_L (x)	385.6			8.8	23.1	68.1
20	30	50	α	380.1			20.0	31.7	48.2
			α_L (x)	387.6			11.4	18.3	70.3
28	36	36	α	380.5			24.2	34.1	41.7
			ε	275.1	443.6	1.612	30.4	34.5	35.1
40	25	35	ε	276.3	443.6	1.605	-	-	-
60	5	35	ε	277.9	445.5	1.603	49.0	6.0	45.0
			β	314.8			90.0	2.4	7.6
75	5	20	ε	277.7	445.1	1.603	49.6	8.0	42.4
			β	314.6			89.3	3.2	7.5

(x) liquid phase at 1700°C

Fig. 5a to c. Microstructures of alloys in the Mo-Rh-Pd system after annealing at 1700 °C. (a) 75 Mo, 5 Rh, 20 Pd (at.%); dark: $\beta + \varepsilon$, bright: ε. (b) 60 Mo, 5 Rh, 35 Pd; dark: β, bright: ε. (c) 20 Mo, 30 Rh, 50 Pd; bright: α, dark phases at grain boundaries: liquid.

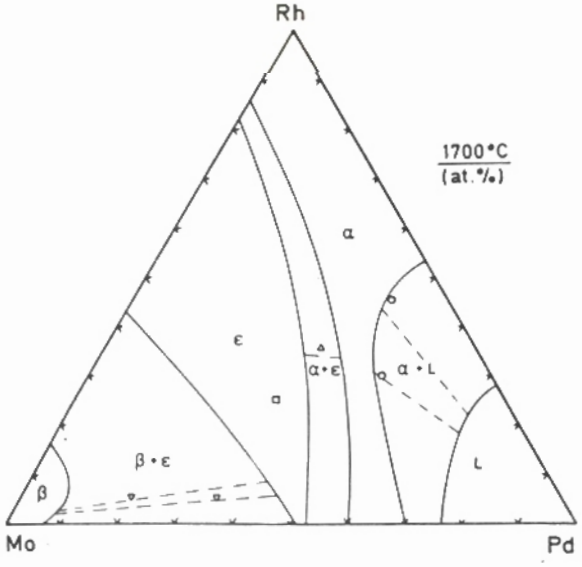

Fig. 6. Isothermal section of the ternary Mo-Rh-Pd system at 1700 °C.

lized ε phase of the binary Mo-Pd system. The curvature of the phase boundary between β and $\beta + \varepsilon$ is unexpected. However, this is supported by precise tie-line evaluations in the $\beta + \varepsilon$ field. The Pd rich region of the ternary system is more complex due to the low melting point of this element at 1555 °C. Owing to Pd losses due to evaporation, this region was not investigated, the phase boundaries are only tentative. The sample with the nominal composition 20 Mo – 20 Ru – 60 Pd (at.%) which clearly revealed three phases (fig. 3d), namely ε, α and L after heat treatment at 1700 °C for 24 h, was selected for the evaluation of the terminal compositions in the three-phase region. Whereas the compositions on the α and ε apices of the triangle could be precisely determined by EPMA, the solidified liquid L showed a large scatter and therefore, a mean value of the L apex in only given. The *c/a* ratio is again markedly increased from 1.583 for pure Ru to 1.607 for the Mo-Pd rich solid solution in equilibrium with the α phase (table 3).

3.3 The ternary Mo-Rh-Pd system

The nominal compositions of the investigated samples as well as the X-ray analysis and the EPMA results are given in table 4. Typical microstructures are illustrated in fig. 5. The unetched bright areas correspond to the ε phase. The Mo rich β phase has a dark appearance in the etched microstructures (figs. 5a and b) as well as the solidified Pd rich liquid which is precipitated as a network in the grain boundaries of the α phase. The location of the tie-lines in fig. 6 does not correspond with that of the nominal compositions due to Pd loss during the heat treatment.

Table 5. Compositions and lattice parameters of phases in the Ru-Rh-Pd system.

nominal comp. in at.%			phases	lattice parameter in pm			EPMA results in at.%		
Ru	Rh	Pd		a	c	c/a	Ru	Rh	Pd
70	15	15	ε	270.7	429.7	1.587	75.2	13.9	10.9
60	10	30	ε	271.0	429.7	1.585	-	-	-
			α	387.9					
55.0	22.5	22.5	ε	271.2	430.9	1.589	63.5	23.2	13.3
			α	384.1			38.0	21.9	40.1
55	10	35	ε	270.7	429.7	1.587	-	-	-
			α	387.9					
45	15	40	ε	271.0	431.1	1.590	67.6	21.3	11.1
			α_L (x)	387.9			6.1	7.9	86.0
40	30	30	ε	271.2	430.0	1.585	52.1	37.1	10.8
			α	383.1			37.6	29.2	33.2
40	15	45	ε	271.2	431.6	1.591	65.5	21.6	12.9
			α_L (x)	387.9			7.2	8.5	84.3
30	35	35	α	382.3			28.2	35.6	36.2
25	30	45	α	383.1			29.1	30.8	40.1
			α_L (x)	-			7.6	12.0	80.4
20	40	40	α	383.1			22.4	40.4	37.2
			α_L (x)	-			5.3	18.9	75.8

(x) liquid phase at 1700°C

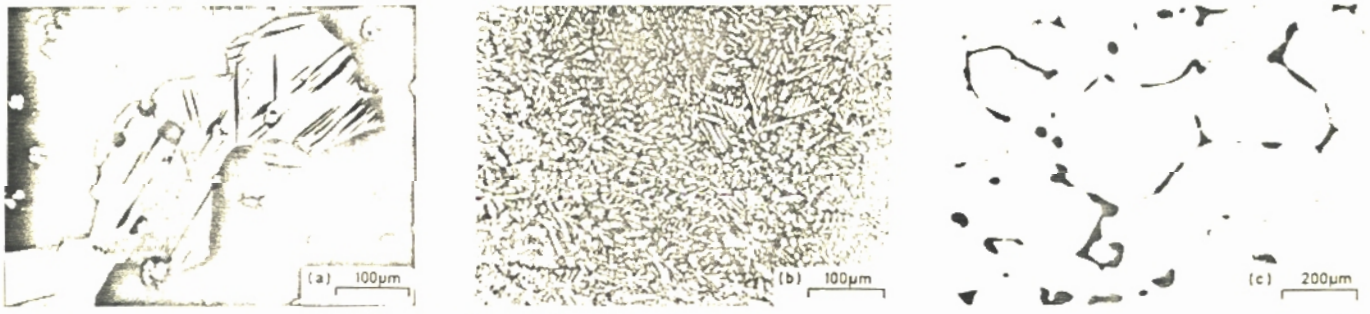

Fig. 7a to c. Microstructures of alloys in the Ru-Rh-Pd system after annealing at 1700 °C. (a) 75.2 Ru, 13.9 Rh, 10.9 Pd (at.%); monophase: ε, Widmannstätten plates (α phase) precipitated during cooling. (b) 55 Ru, 22.5 Rh, 22.5 Pd; dark: α, bright: ε. (c) 25 Ru, 30 Rh, 45 Pd; bright: α, dark phases at grain boundaries: liquid.

The isothermal section of the ternary Mo-Rh-Pd system at 1700 °C is given in fig. 6. It is characterized by two continuous solid solution regions. No hexagonal element is component of the ternary Mo-Rh-Pd system. However, intermediate hexagonal phases are stabilized in the binary Mo-Rh system between 43 and 82 at.% Rh[23)25)26)] and in the binary Mo-Pd system between 51 and 53 at.% Pd[28)] which form a continuous solid solution in the ternary system. Complete miscibility further exists between Rh and the α region of the binary Mo-Pd system which amounts to about 60 to 70 at.% Pd at 1700 °C. The fcc solid solution in the ternary system is extended to the Pd apex in the temperature range of complete Rh-Pd miscibility below 1555 °C.

3.4 The ternary Ru-Rh-Pd system

The nominal compositions of the investigated samples as well as the X-ray analysis and the EPMA results are given in table 5. Representative microstructures are illustrated in fig. 7. Figure 7a depicts the microstructure of the ε region under polarized light with Widmannstätten plates (α phase) precipitated during cooling. The Ru rich ε phase is bright, the Rh rich α phase is dark in appearance in the etched two-phase microstructure (fig. 7b). Figure 7c reveals the α phase and the solidified liquid as dark phase at the grain boundaries.

The isothermal section of the ternary Ru-Rh-Pd system at 1700 °C is given in fig. 8. It is characterized by three exten-

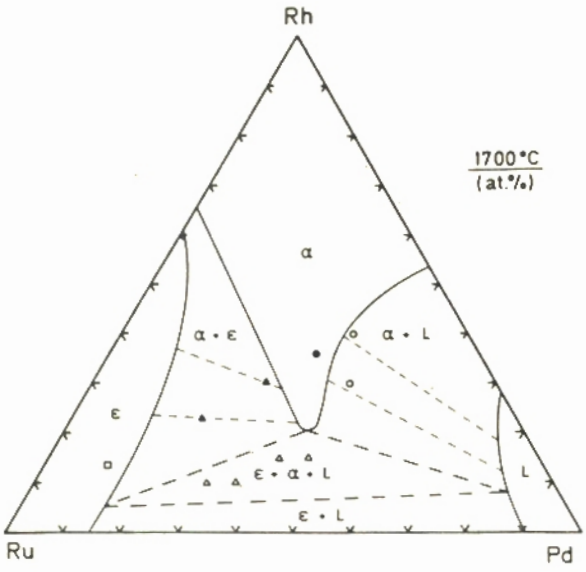

Fig. 8. Isothermal section of the ternary Ru-Rh-Pd system at 1700 °C.

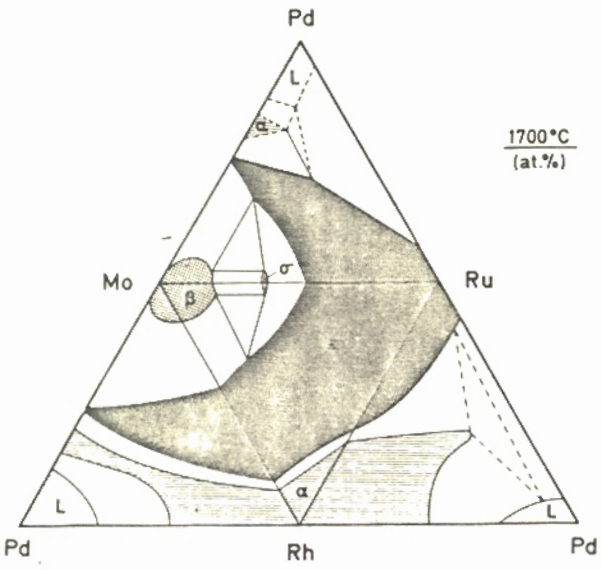

Fig. 9. Isothermal ternary sections in the quaternary Mo-Ru-Rh-Pd system at 1700 °C.

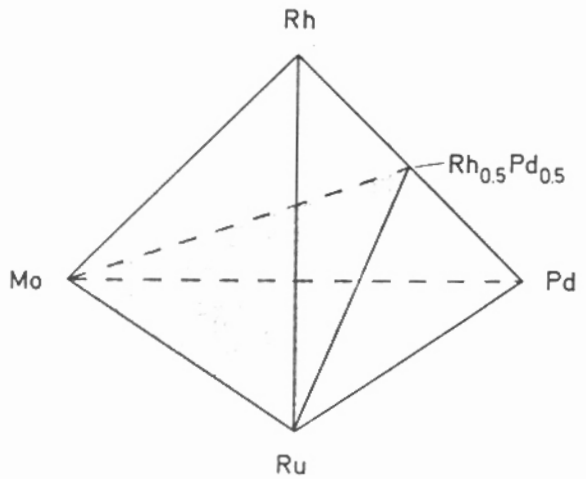

Fig. 10. Location of the isothermal pseudoternary Mo-Ru-$Rh_{0.5}Pd_{0.5}$ section in the quaternary Mo-Ru-Rh-Pd system.

sive mono-phase regions α, ε and L originating from the pure elements and one three-phase field between them. The tie-lines in the Pd rich two-phase region determined by EPMA do not agree with the nominal compositions due to material loss during heat treatment. The apices in the three-phases $\alpha + \varepsilon + L$ region could not be determined precisely on account of insufficient quality of the microstructures and large scatter in the composition of the phases obtained by EPMA. The homogeneity range of the Rh(Ru,Pd) solid solution (α phase) is strongly increased by Ru and Pd additions. Rh can dissolve up to 80 at.% $Ru_{0.5}Pd_{0.5}$ in equimolar composition at 1700 °C without any change of the fcc structure of the host lattice.

3.5 The quaternary Mo-Ru-Rh-Pd system

The four isothermal sections of the ternary systems, Mo-Ru-Rh, Mo-Ru-Pd, Mo-Rh-Pd and Ru-Rh-Pd, at 1700 °C are arranged in fig. 9 as four interconnected Gibbs triangles which form the surface of the tetrahedron of the quaternary system.

One of the objectives of this study was the elaboration of the pseudo-ternary section with Mo and Ru as pure components and Rh and Pd in a constant ratio as the third component. It is known from studies on irradiated oxide fuels that these elements and Tc form quinary fission product precipitates. It is supposed that the crystal chemical behaviour of Tc in this quinary system is very similar to that of Ru; hence, the reduction of this system to a quaternary one is defendable. Both the fcc fission products Rh and Pd are generated in lower yields. A Rh/Pd ratio equal to unity was decided for further reduction to a ternary system; the location of the pseudoternary section Mo-Ru-$Rh_{0.5}Pd_{0.5}$ in the quaternary system is illustrated in fig. 10. This presentation is presumably the most qualified one for figuring the complex alloying behaviour of the quaternary system in a two-dimensional form.

The nominal compositions of the investigated samples of the pseudoternary Mo-Ru-$Rh_{0.5}Pd_{0.5}$ section as well as the X-ray analysis and the EPMA results are summarized in table 6. Typical microstructures are given in fig. 11. Examples from the two-phase $\beta + \varepsilon$, $\sigma + \varepsilon$ and $\alpha + \varepsilon$ regions are illustrated in figs. 11a to d. The microstructure of the σ phase which is dark in appearance after chemical etching (fig. 11b) has been additionally gas-etched giving light appearance under polarized light (fig. 11c); the black regions are products of decomposed σ or ε phase. Figs. 11e and f give examples from the three-phase $\beta + \sigma + \varepsilon$ regions; fig. 11f shows a pronounced decomposition of the ε phase in the dark regions.

The isothermal pseudoternary Mo-Ru-$Rh_{0.5}Pd_{0.5}$ section of the quaternary Mo-Ru-Rh-Pd system at 1700 °C is illustrated in fig. 12. The different symbols denote nominal compositions or those obtained by EPMA if the respective sample has been analyzed (see table 6). The hexagonal ε phase appears like in the corresponding ternary systems in a broad concentration range. Complete miscibility exists between ε-Ru(Mo,$Rh_{0.5}Pd_{0.5}$) and the intermediate ε-[Mo-$Rh_{0.5}Pd_{0.5}$] phase. The measured lattice parameters *a* and *c* of the samples within the mono-phase ε region have been fitted, they are given as iso-lattice parameter curves for values of *a* between 271 and 276 pm in fig. 13 and for values of *c* between 430 and 444 pm in fig. 14. Neither *a* and *c* are linear with concentration along the Ru-$Mo_{0.5}Rh_{0.25}Pd_{0.25}$ section nor the *c*/*a* ratio is constant. The same non-linearity holds for the binary Ru-Mo[23,24] and Ru-Rh[16] sys-

Table 6. Compositions and lattice parameters of phases in the Mo-Ru-Rh-Pd system.

nominal comp. in at.%				phases	lattice parameters in pm			EPMA results in at.%			
Mo	Ru	Rh	Pd		a	c	c/a	Mo	Ru	Rh	Pd
5	60	17.5	17.5	ε	271.6	432.4	1.592	-	-	-	-
				α	385.7						
10	63	13.5	13.5	ε	272.2	432.6	1.590	9.5	64.1	14.9	11.5
10	70	10	10	ε	272.2	432.2	1.588	-	-	-	-
10	30	30	30	ε	272.3	434.7	1.596	-	-	-	-
10	20	35	35	α	384.8			-	-	-	-
15	40	22.5	22.5	ε	273.3	436.3	1.596	-	-	-	-
				α	385.9			-	-	-	-
15	50	17.5	17.5	ε	273.4	435.9	1.594	-	-	-	-
15	10	37.5	37.5	α	385.5			13.5	9.5	35.1	41.9
20	20	30	30	ε	273.8	438.7	1.602	-	-	-	-
				α	385.4			-	-	-	-
20	50	15	15	ε	273.8	436.0	1.592	-	-	-	-
20	56	12	12	ε	273.0	433.7	1.589	20.6	55.6	13.1	10.7
25	5	35	35	ε	275.1	439.7	1.598	-	-	-	-
				α	385.5			-	-	-	-
25	35	20	20	ε	274.3	437.9	1.596	-	-	-	-
25	25	25	25	ε	274.4	439.1	1.600	-	-	-	-
30	40	15	15	ε	274.8	439.0	1.597	27.9	41.2	15.4	15.5
30	10	30	30	ε	275.5	443.0	1.611	29.0	10.0	29.5	31.5
30	49	10.5	10.5	ε	274.7	435.5	1.593	29.2	49.0	10.4	11.4
35	35	15	15	ε	275.6	442.5	1.606	-	-	-	-
35	5	30	30	ε	275.7	442.5	1.605	-	-	-	-
40	42	9	9	ε	275.3	442.1	1.606	38.0	44.0	9.4	8.6
40	20	20	20	ε	276.0	443.2	1.606	42.3	20.3	19.7	17.7
45	45	5	5	ε	275.5	442.6	1.606	43.1	47.0	5.4	4.5
45	38.5	8.25	8.25	ε	275.6	443.2	1.608	43.6	39.4	9.0	8.0
45	5	25	25	ε	276.7	445.6	1.610	44.6	5.2	24.2	25.7
48.6	36.0	7.7	7.7	ε	276.5	444.9	1.609	-	-	-	-
				σ	957.1	494.2	0.516	-	-	-	-
48.5	31.5	10.0	10.0	ε	276.4	445.2	1.611	-	-	-	-
				σ	956.0	493.9	0.517	-	-	-	-
50	10	20	20	ε	276.4	444.4	1.608	49.9	10.1	19.3	20.7
50	40	5	5	ε	276.3	444.4	1.608	46.6	42.7	6.1	4.6
				σ	956.0	494.7	0.517	-	-	-	-
50	20	15	15	ε	276.4	443.9	1.606	-	-	-	-
54	21	12.5	12.5	ε	276.7	444.1	1.605	51.6	20.6	13.8	14.0
				β	313.6			75.5	14.2	6.0	4.3
				σ +				-	-	-	-
55	40	2.5	2.5	ε	275.8	443.9	1.609	-	-	-	-
				σ	956.0	494.1	0.517	-	-	-	-
55	31.6	6.7	6.7	ε	276.4	443.0	1.603	52.2	29.8	9.8	8.2
				β	313.0			76.2	18.3	2.7	2.8
				σ	956.6	493.8	0.516	-	-	-	-
55	10	17.5	17.5	ε	277.3	445.1	1.605	-	-	-	-
				β	314.5						

Continued Table 6

nominal comp. in at.%				phases	lattice parameters in pm			EPMA results in at.%			
Mo	Ru	Rh	Pd		a	c	c/a	Mo	Ru	Rh	Pd
60	35	2.5	2.5	ε	276.4	442.6	1.601	48.0	43.9	4.2	3.9
				σ	956.3	494.3	0.517	61.1	34.5	2.7	1.7
60	28	6	6	ε	276.3	443.8	1.606	-	-	-	-
				β	313.6			-	-	-	-
				σ	957.7	494.6	0.516	-	-	-	-
60	5	17.5	17.5	ε	277.6	445.5	1.605	-	-	-	-
				β	314.1			-	-	-	-
63	32	2.5	2.5	ε	276.0	442.4	1.603	-	-	-	-
				β	313.4			-	-	-	-
				σ	954.7	495.4	0.519	-	-	-	-
65	20	7.5	7.5	ε	276.1	443.2	1.605	51.6	25.8	13.6	9.0
				β	313.4			72.7	18.9	5.9	2.5
				σ	957.3	495.1	0.517	-	-	-	-
65	10	12.5	12.5	ε	276.4	443.5	1.605	52.8	13.9	19.9	12.3
				β	313.7			80.8	8.2	7.2	3.8
70	21	4.5	4.5	ε	276.0	443.1	1.605	-	-	-	-
				β	313.3			-	-	-	-
				σ*	959.3	497.8	0.519	-	-	-	-
70	15	7.5	7.5	ε	276.2	443.2	1.605	-	-	-	-
				β	313.4			-	-	-	-
70	10	10	10	ε	276.9	445.6	1.609	52.5	13.6	16.8	17.1
				β	313.8			80.4	8.8	6.3	4.5
70	5	12.5	12.5	ε	277.0	446.6	1.612	-	-	-	-
				β	313.9			-	-	-	-
73	20	3.5	3.5	ε	275.9	444.0	1.609	-	-	-	-
				β	313.3			-	-	-	-
73	15	6	6	ε	276.4	445.2	1.611	-	-	-	-
				β	313.4			-	-	-	-
73	7	10	10	ε	276.4	445.8	1.613	-	-	-	-
				β	313.8			-	-	-	-
75	20	2.5	2.5	ε	276.3	444.0	1.607	-	-	-	-
				β	313.8			-	-	-	-
				σ +				-	-	-	-
75	15	5	5	ε	275.9	443.9	1.609	-	-	-	-
				β	313.7			-	-	-	-
75	10	7.5	7.5	ε	276.8	443.8	1.603	-	-	-	-
				β	313.5			-	-	-	-
75	5	10	10	ε	276.3	444.1	1.607	52.1	6.8	18.7	22.4
				β	313.9			80.1	4.7	8.4	6.8
80	10	5	5	ε	276.9	444.6	1.606	-	-	-	-
				β	313.8			-	-	-	-
80	14	3	3	β	313.0			-	-	-	-
85	10	2.5	2.5	β	313.5			-	-	-	-
85	5	5	5	β	313.7			-	-	-	-

* lattice parameters calculated from two reflections

\+ only one reflection

tems. Either Rh and Pd or both elements stabilize Mo_5Ru_3 in the Mo-Ru system. The simultaneous addition of Rh and Pd has shown the same effect on the stabilization of the tetragonal σ phase in the quaternary system. There exists no four-phase field in the pseudoternary section. The three-phase field $\beta + \sigma + \varepsilon$ has a curved boundary adjacent to the $\sigma + \varepsilon$ field of the Mo-Ru-$Rh_{0.5}Pd_{0.5}$ section.

Microhardness measurements have been made at room temperature on all embedded samples of the pseudoter-

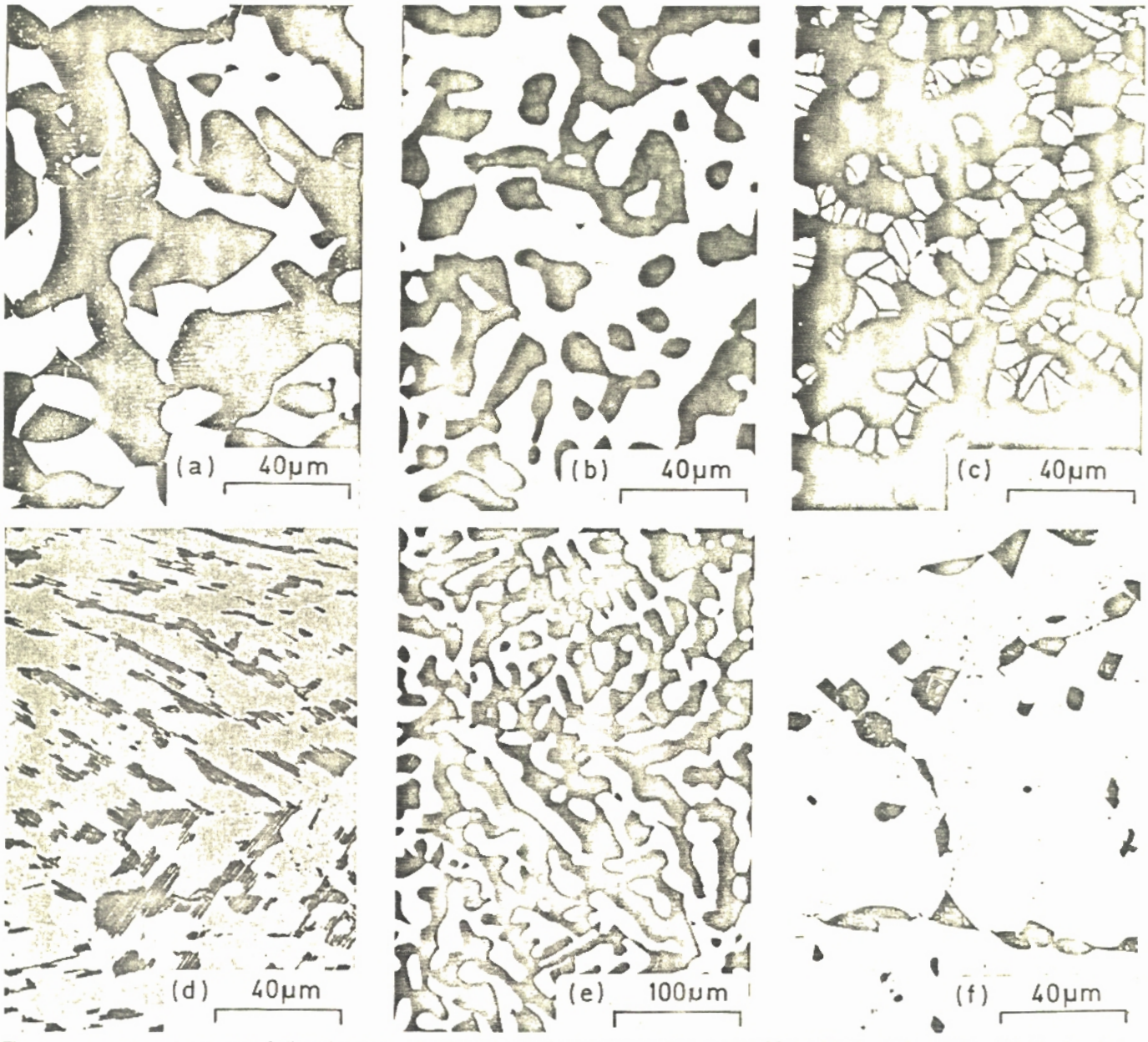

Fig. 11a to f. Microstructures of alloys in the Mo-Ru-Rh-Pd system after annealing at 1700 °C. (a) 70 Mo, 10 Ru, 10 Rh, 10 Pd (at.%); dark: $\varepsilon+\beta$, bright: ε. (b) 55 Mo, 40 Ru, 2.5 Rh, 2.5 Pd; dark: σ, bright: ε. (c) 55 Mo, 40 Ru, 2.5 Rh, 2.5 Pd; bright: σ, grey: ε, black: decomposition of σ or ε. (d) 15 Mo, 40 Ru, 22.5 Rh, 22.5 Pd; dark: α, grey: ε. (e) 63 Mo, 32 Ru, 2.5 Rh, 2.5 Pd; dark: $\beta+\sigma$, bright: ε, σ observed by X-ray diffraction. (f) 55 Mo, 31.6 Ru, 6.7 Rh, 6.7 Pd; dark phases at grain boundaries: $\beta+\varepsilon$, bright: ε, grey: decomposition of ε, σ observed by X-ray diffraction.

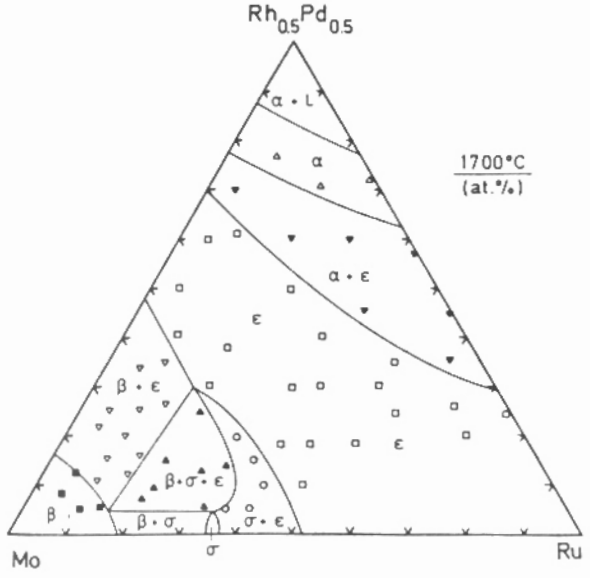

nary section using 1 N load. The hardness results given in fig. 15 are averaged values of at least 20 measurements for each composition in the different phase fields. The samples of compositions close to the $\varepsilon/\varepsilon+\alpha$ phase boundary are very brittle. The experimental results are fitted and are given as 500 HV and 600 HV iso-microhardness curves. In particular, the mono-phase ε region can be classified into three microhardness regions: $<$ 500 HV, 500 to 600 HV and $>$ 600 HV.

The knowledge of the microhardness and the lattice parameters of samples within the mono-phase ε-region renders informations on the chemical composition of the phases without any direct chemical analysis.

Fig. 12. Isothermal pseudoternary Mo-Ru-$Rh_{0.5}Pd_{0.5}$ section of the quaternary Mo-Ru-Rh-Pd system at 1700 °C.

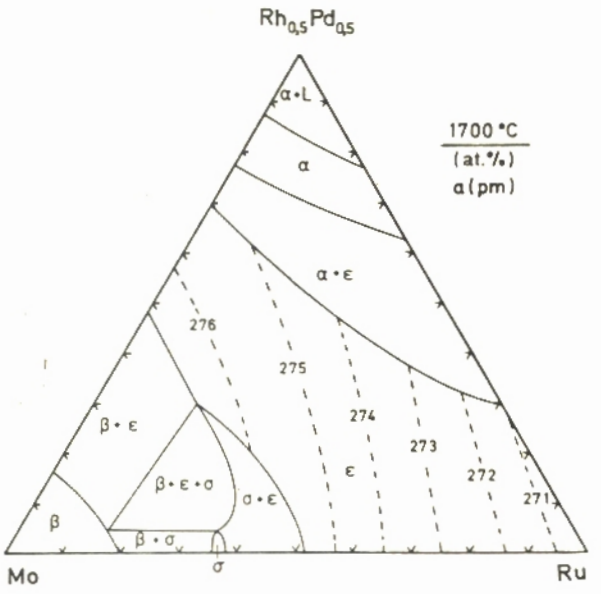

Fig. 13. Constant lattice parameter curves (*a* in pm) of the hexagonal ε phase in the pseudoternary Mo-Ru-$Rh_{0.5}Pd_{0.5}$ section of the quaternary Mo-Ru-Rh-Pd system.

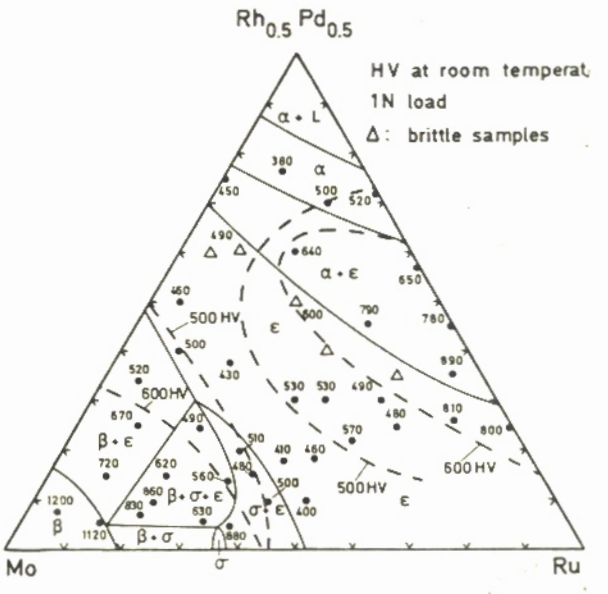

Fig. 15. Room temperature iso-microhardness curves (500 HV and 600 HV) in the pseudoternary Mo-Ru-$Rh_{0.5}Pd_{0.5}$ section of the quaternary Mo-Ru-Rh-Pd system.

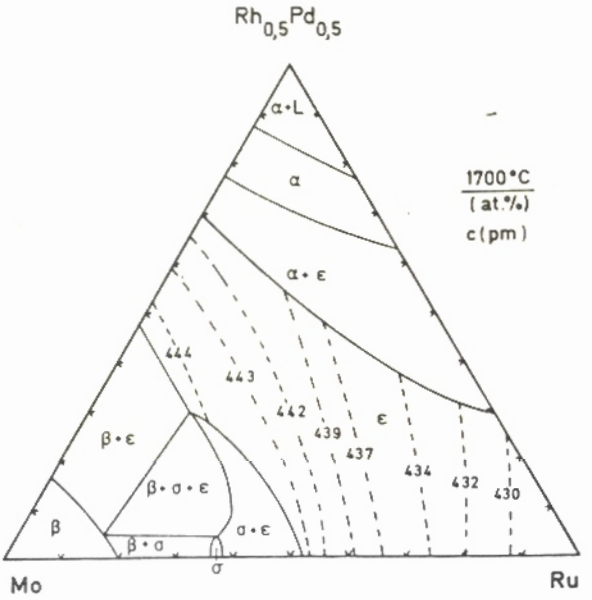

Fig. 14. Constant lattice parameter curves (*c* in pm) of the hexagonal ε phase in the pseudoternary Mo-Ru-$Rh_{0.5}Pd_{0.5}$ section of the quaternary Mo-Ru-Rh-Pd system.

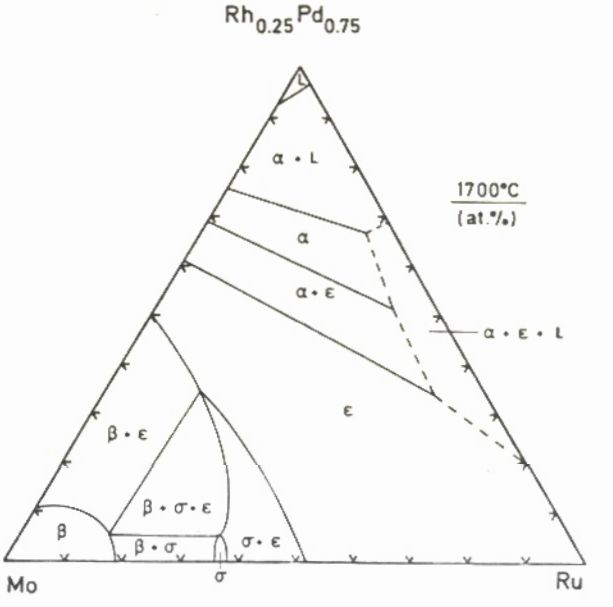

Fig. 16. Interpolated isothermal pseudoternary Mo-Ru-$Rh_{0.25}Pd_{0.75}$ section of the quaternary Mo-Ru-Rh-Pd system at 1700 °C.

Two further pseudoternary sections of the quaternary system, Mo-Ru-($Rh_{0.25}Pd_{0.75}$) and Mo-Ru-($Rh_{0.75}Pd_{0.25}$), are proposed by interpolation of the investigated ternary sections Mo-Ru-Rh, Mo-Ru-Pd, Mo-Rh-Pd and Ru-Rh-Pd and the pseudoternary section Mo-Ru-($Rh_{0.5}Pd_{0.5}$). These isothermal sections at 1700 °C are represented in figs. 16 and 17.

The quaternary Mo-Ru-Rh-Pd system at 1700 °C is characterized by the existence of two extended mono-phase state spaces. The hexagonal closed packed ε space permeates the entire concentration tetrahedron whereas the α space is cut off by the Pd rich liquid. The occurrence of the σ phase up to about 1900 °C and the Pd rich melt above 1555 °C is reason for two prismoidal three-phase spaces, $\beta+\sigma+\varepsilon$ and $\varepsilon+\alpha+L$, with two areas of intersection each with the respective surfaces of the concentration tetrahedron. There is no four-phase space in the quaternary system at 1700 °C.

4. Conclusions

Molybdenum, technetium, ruthenium, rhodium and palladium are generated in high yield during nuclear fission. These fission products form mono- or two-phase metallic precipitates in irradiated uranium-plutonium oxide. Postirradiation studies have shown that the composition is dependent on the oxygen partial pressure of the fuel in

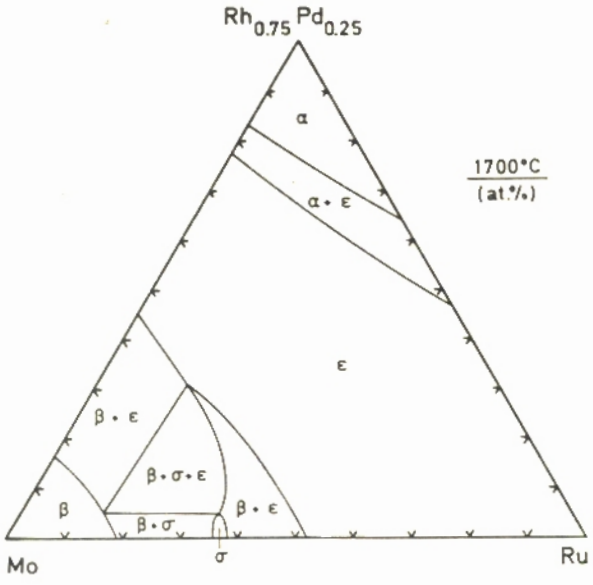

Fig. 17. Interpolated isothermal pseudoternary Mo-Ru-$Rh_{0.75}Pd_{0.25}$ section of the quaternary Mo-Ru-Rh-Pd system at 1700 °C.

the end of irradiation and on the temperature gradients of the fuel pins. The crystal structure is mainly hexagonal. The compositions cover the pseudobinary section Mo-$(Tc,Ru)_{0.7}(Rh,Pd)_{0.3}$ in the corresponding quinary system. As the completely miscible hexagonal elements Tc and Ru are considered to be equivalent in the crystal chemical sense, the alloying behaviour and the crystal structure of the in-pile observed fission product precipitates can be interpreted on the basis of the results of the quaternary Mo-Ru-Rh-Pd system. The mono-phase hexagonal precipitates become two-phase in two cases:

(1) High Mo contents result in the formation of a second phase: σ or β at temperatures below or above 1900 °C, resp.

(2) Low Mo contents at very high burnups and high Pd contents in the cold fuel regions result in the formation of the α phase as the second phase.

Indeed, these two-phase inclusions have been found in fast breeder reactor fuels at very high burnups above 10 % of the actinides and in all oxide fuel pins with the entire Mo inventory in the metallic state at very low oxygen partial pressures.

The authors gratefully acknowledge the assistance of Mr. W. Laumer and Mr. H. Späte in conducting the experiments.

Literature

1) B. T. BRADBURY, J. T. DEMAND, P. M. MARTIN, and D. M. POOLE, J. Nucl. Mat. **17** (1965) 227.
2) B. M. JEFFERY, J. Nucl. Mat. **22** (1967) 33.
3) J. I. BRAMMAN, R. M. SHARPE, D. THOM, and G. YATES, J. Nucl. Mat. **25** (1968) 201.
4) D. R. O'BOYLE, F. L. BROWN, and J. E. SANECKI, J. Nucl. Mat. **29** (1969) 27.
5) H. KLEYKAMP, in Proc. IAEA Panel on Behaviour and Chemical State of Irradiated Ceramic Fuels, Vienna (1972) 157.
6) H. HOLLECK and H. KLEYKAMP, reports KfK 1181 (1970) and EURFNR 836 (1970).
7) I. JOHNSON, C. E. JOHNSON, C. E. CROUTHAMEL, and C. A. SEILS, J. Nucl. Mat. **48** (1973) 21.
8) H. KLEYKAMP, J. Nucl. Mat. **66** (1977) 292.
9) F. THÜMMLER, H. KLEYKAMP, and P. HOFMANN, J. Nucl. Mat. **81** (1979) 215.
10) R. FÖRTHMANN, H. GRÜBMEIER, H. KLEYKAMP, and A. NAOUMIDIS, in Proc. IAEA Symp. on Thermodyn. of Nucl. Mater., Vol. I, Vienna (1974) 147.
11) H. KLEYKAMP, report KfK 2213 (1975).
12) H. KLEYKAMP, J. Nucl. Mat. **84** (1979) 109.
13) H. KLEYKAMP, in Proc. Symp. Reaktortagung Mannheim, Kerntechn. Gesellsch. (1977) 510.
14) R. P. ELLIOTT, Constitution of Binary Alloys, First Supplement, McGraw-Hill, New York (1965).
15) F. A. SHUNK, Constitution of Binary Alloys, Second Supplement, McGraw-Hill, New York (1969)
16) J. O. A. PASCHOAL, report KfK 3473 (1983).
17) J. B. DARBY, D. J. LAM. L. J. NORTON, and J. W. DOWNEY, J. Less-Common Metals **4** (1962) 558.
18) J. B. DARBY, L. J. NORTON, and J. W. DOWNEY, J. Less-Common Metals **5** (1963) 397.
19) H. R. HAINES, P. E. POTTER, and M. H. RAND, in Proc. IAEA Symp. on Thermodyn. of Nucl. Mater., Vol. I, Jülich (1979) 471.
20) M. H. RAND, and P. E. POTTER, Physica **103 B** (1981) 21.
21) M. YAMAWAKI, Y. NAGAI, T. KOGAI, and M. KANNO, in Proc. IAEA Symp. on Thermodyn. of Nucl. Mater., Vol. I, Jülich (1979) 249.
22) LANDOLT-BÖRNSTEIN, N. S., Group III, Vol. 6, Springer, Berlin (1971).
23) E. RAUB, Z. Metallkde. **45** (1954) 23.
24) E. ANDERSON and W. HUME-ROTHERY, J. Less-Common Metals **2** (1960) 443.
25) C. W. HAWORTH and W. HUME-ROTHERY, J. Inst. Met. **87** (1958–1959) 265.
26) E. ANDERSON and W. HUME-ROTHERY, J. Less-Common Metals **2** (1960) 19.
27) C. W. HAWORTH and W. HUME-ROTHERY, Phil. Mag. **3** (1958) 1013.
28) E. ANDERSON, J. Less-Common Metals **6** (1964) 81.
29) J. O. A. PASCHOAL, H. KLEYKAMP and F. THÜMMLER, J. Less-Common Metals, in print.
30) B. F. KIEFFER and K. SEDLATSCHEK, in High Temp. Refr. Met., Proc. Metall. Soc. Conf., New York 1965, Vol. 34, Part I, p. 441.
31) E. M. SOKOLOVSKAYA, S. V. KABANOV, M. V. RAYEVSKAYA, and I. G. SOLOKOVA, Russian Metallurgy **5** (1978) 178.
32) A. A. RUDNITSKII and R. S. POLYAKOVA, Russian J. Inorg. Chem. **4** (1959) 631.
33) A. S. DARLING and J. M. YORKE, Plat. Met. Rev. **4** (1960) 104.

(Eingegangen am 27. April 1983)